IOP PUBLISHING JOURNAL OF PHYSICS D: APPLIED PHYSICS

J. Phys. D: Appl. Phys. **44** (2011) 205402 (7pp) doi:10.1088/0022-3727/44/20/205402

Understanding and improving electroluminescence in mill-ground ZnS : Cu,Cl phosphors

S Medling, C France, B Balaban, M Kozina, Y Jiang, F Bridges and S A Carter

Physics Department, University of California, Santa Cruz, CA 95064, USA

E-mail: smedling@ucsc.edu

Received 10 February 2011, in final form 30 March 2011
Published 28 April 2011
Online at stacks.iop.org/JPhysD/44/205402

Abstract

We demonstrate that lightly milled ZnS : Cu,Cl phosphors produce AC electroluminescence (EL) emission in devices half as thick and produce up to 5 times the light output as the thinnest devices made with unground phosphors. We also establish minimum and maximum bounds on micro-milling conditions for producing powders that are still viable for AC EL. To understand the cause of the minimum size, we report extended x-ray absorption fine structure (EXAFS) measurements on phosphors sorted by particle size. The EXAFS data show that grinding preferentially damages the initially embedded CuS nano-precipitate. This suggests that grinding cleaves the ZnS : Cu through the embedded CuS nano-precipitates, leaving the CuS nano-precipitates on the surface to be further broken apart by continued grinding, eventually reducing the effectiveness of the CuS-induced electric field enhancement.

(Some figures in this article are in colour only in the electronic version)

1. Introduction

Activated ZnS phosphor powders have been studied for solid-state lighting applications since Destriau discovered their electroluminescence (EL) under AC excitation [1]. Extensive research culminated in the best experimental observations and mechanistic theory by Fischer in 1963 [2, 3]. Fischer observed that light emission was in the form of alternating emission from either end of a linear structure within the individual ZnS : Cu,X phosphor particles. At Cu concentrations above $\sim$0.04%, it is proposed that most of the Cu precipitates out along [1 1 1] crystal imperfections or grain boundaries during the cooling phase of fabrication. These conducting CuS inclusions have a needle or disc like shape that causes an electic field enhancement of up to 100$\times$ near the ends, allowing field-emission of charge carriers from the CuS to trap states within the ZnS host where radiative recombination occurs [4–6]. This results in tiny, bright emission points within the phosphors, as shown in figure 1. Though AC EL occurs at average applied field strengths two orders of magnitude below DC EL, typical commercial phosphors (made with particles 20–30 μm in diameter) still require several hundred volts peak-to-peak for full efficiency.

A simple means to decrease the required applied voltage would be to decrease the film thickness, but requires smaller powder particles. Though AC thin-film EL has been studied extensively [7] and nanoparticle AC EL devices have recently been reported [8], neither of these technologies utilizes the local electric field enhancements found in ZnS : Cu,Cl powder AC EL devices. Currently available AC EL ZnS : Cu,Cl phosphor particles can be milled to produce smaller phosphor particles in an attempt to allow thinner AC EL devices that still contain field enhancements from the CuS nano-precipitates [9]. Here we show that good EL at somewhat lower voltages is possible, but thin films made using heavily ground ZnS : Cu,Cl particles have a very weak output. Moreover, when the powder particles were size sorted, no significant EL output ($<$1%) was observed for the particles $\leqslant$2 μm in size.

To understand these changes in the EL output with decreasing particle size we have carried out extended x-ray absorption fine structure (EXAFS) measurements to probe any significant disorder in the ZnS : Cu,Cl particles as a result of grinding. We show that for the size selected particles there is a large increase in the disorder about the Cu sites but no observable change in the disorder about the Zn atoms in the ZnS lattice.

 © 2011 IOP Publishing Ltd Printed in the UK & the USA

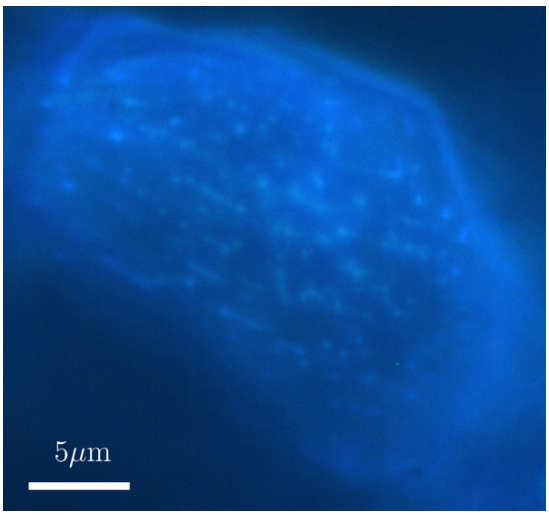

Figure 1. A 20 μm particle with the individual emission centres visible.

2. EL studies

Commercially available EL ZnS : Cu,Cl phosphor powders were milled using a FRITSCH Pulverisette 7 planetary micro-mill with 5 mm hardened steel beads. To ensure minimal thermal degradation, all milling was carried out in multiple cycles, with each cycle shorter than 2 min and an equal rest cycle between cycles. Ac EL devices were fabricated using as-made and milled commercially available blue–green emitting ZnS : Cu,Cl phosphor from Osram-Sylvania (GGL21, GGS22) and Osram-Sylvania EL binder with a superstrate device structure on indium tin oxide (ITO) patterned glass, see figure 2 inset. Phosphor material was mixed with binder by mass at a ratio of $m_{\rm ph}/m_{\rm bi} = 0.55 \pm 0.02$, and doctor bladed onto ITO patterned glass slides using a razor blade. Two pieces of tape or thin Mylar were used to control the wet film thickness. Slides were annealed in a vacuum oven at 110 °C and ∼1 Torr for 30 min. A silver top electrode was applied perpendicularly to the lower ITO electrode using similar methods as used to prepare the phosphor layer. Completed active device area was 3.0 mm by 6.4 mm.

Room temperature photoluminescence (PL) measurements were made on films deposited on glass slides using a Perkin-Elmer LS45 spectrophotometer. The set-up for PL collected a small solid angle of the fluorescence emission and provided a reproducible shape for the spectra; however, the amplitude was quite sensitive to scattering from the sample surface and varied considerably as the sample was changed or moved. For AC EL, the devices were driven by a HP 3245A power supply with sinusoidal waveforms, while light output was measured either by an Ocean Optics SD2000 optical spectrometer for spectral information or by a Si photodiode connected to a Keithly 425 Picoammeter for automated frequency or voltage sweeps. In this case an optical fibre was placed close to the device under measurement and collected the emission from a large fraction of the subtended solid angle; for this set-up, the output was relatively insensitive to small motions of the sample and relative intensity measurements were reproducible to a few per cent. Also note that under AC operation, the devices are nearly perfect capacitors and we were not able to reliably measure the in-phase current (even using lock-in techniques); hence we cannot provide an estimate of the power efficiency.

Table 1. Summary of EL results for various micro-milled ZnS : Cu,Cl phosphors. The relative EL intensity was obtained by comparing photodiode current at 160 $V_{\rm pp}$ excitation for the as-ground material.

Phosphor	Speed (RPM)	Time (min)	EL Int. (%)
GGL21	200	2	86
GGL21	400	2	16
GGL21	400	4	2
GGL21	400	8	3
GGS22	100	10	100
GGS22	200	2	86

Dry film thicknesses of phosphor layers were measured to an accuracy of ± 5 μm before Ag contact deposition with a vernier micrometer and averaging over several locations on the device. Scanning electron microscope images of phosphor powders were obtained using an ISI WB-6 SEM.

Micro-milling was carried out on short (GGS22) and long (GGL21) lifetime Osram-Sylvania ZnS : Cu,Cl blue–green emitting phosphors at milling speeds from 100 to 400 RPM. The effects of milling on emission intensities are summarized in table 1. Both the GGL21 and GGS22 phosphors showed similar behaviour after milling, with the EL and PL emission shapes unchanged, as seen in figure 2. Milling speeds of 100 RPM produced minimal effects on phosphor powder. The powder's visual appearance, EL emission and PL emission were virtually unchanged. Milling speeds of 400 RPM produced a very fine, sticky powder. These powders showed a significant decrease in PL and EL emission. Milling either phosphor at 200 RPM for 2 min produced a powder with a finer consistency than as-made, yet still retained significant PL and EL emission. Figure 3 inset shows SEM images of GGS22 phosphors milled at 200 RPM. Lightly milled phosphors (left) still have smooth crystal surfaces while strongly milled phosphors (right) show rough damaged surfaces and many small fragments.

Figure 3 shows relative AC EL luminance for as-made and two different milled samples of GGL21. For similarly prepared devices the AC EL luminance after 2 min at 200 RPM milling is on average 75% that of the as-made phosphor while after 4 min at 400 RPM milling the intensity is on average 2%. Optimal devices were fabricated with as-made phosphor using a single layer of 3M Scotch® 810 Magic tape to set wet film thickness. After subsequent annealing, dry film thicknesses were measured to be 58 ± 5 μm. Attempts were made to produce thinner devices with as-made particles using 25 μm Mylar®, but these devices were electrically shorted or had non-uniform films. However, using milled particles (GGL21, 2 min, 200 RPM), but not size-sorted, thinner devices were successfully fabricated. Figure 4 shows AC EL intensities for three thicknesses of devices produced with milled phosphor and optimal as-made phosphor. Gains of nearly a factor of 5 were obtained for a 25 μm thick device from milled particles compared to a 58 μm device of as-made particles for 40 $V_{\rm pp}$,

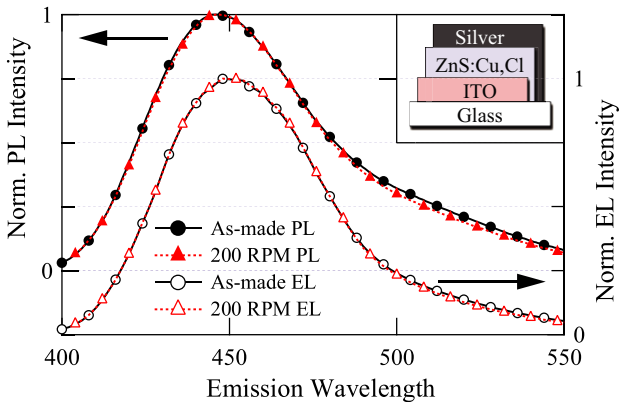

Figure 2. Left/filled markers: Normalized PL emission spectra under 325 nm excitation for GGL21 phosphor as-made (solid circles) and after 2 min of 200 RPM milling (dashed triangles). Right/open markers: Normalized EL emission from 80 kHz, 200 V_{pp}, for same phosphors. Inset: AC EL device structure.

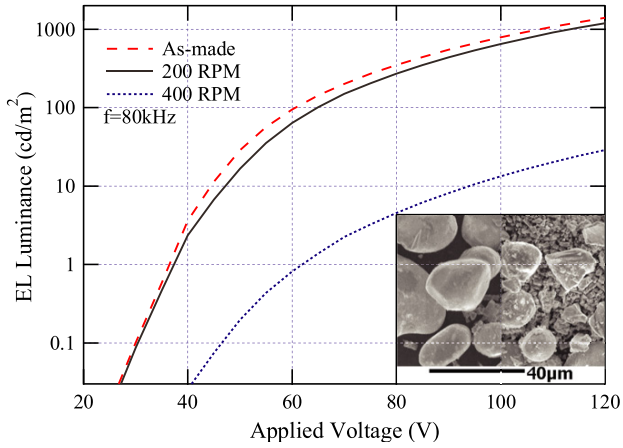

Figure 3. EL luminance for 58 μm thick devices under 80 kHz excitation for GGL21 phosphor as-made (dashed line), after 2 min of 200 RPM milling (solid line), and after 4 min of 400 RPM milling (dotted line). Inset: SEM images of a lightly (left) and strongly (right) ground GGS22 phosphors.

20 kHz excitation. This emission gain at low voltages was robust across frequencies of 200 Hz–80 kHz excitations, as shown in figure 5, but output of the as-made device approached that of the thinnest milled device as the driving voltage exceeded 100 V_{pp}, shown in figure 4 inset.

It is not clear why there is such a significant decrease in AC EL for the smallest particles, particularly when AC EL has been observed for nanoparticles of ZnS [8], though the emission mechanism might be different. To reduce the AC EL intensity either (1) the emission centres—electron traps on Cl^{-1} and hole traps on complex Cu centres—are damaged during grinding, (2) the CuS needle-like precipitates are damaged, diminishing the local E-field enhancement, (3) both (1) and (2) occur, or (4) the size of the host ZnS particle plays an unknown but significant role. We address possible grinding-induced disorder in the next section. In addition, the PL was consistently lower for ground samples although our set-up did not allow a good quantitative measure of the spatially integrated intensity. We address possible reasons for a reduction in PL in the discussion section.

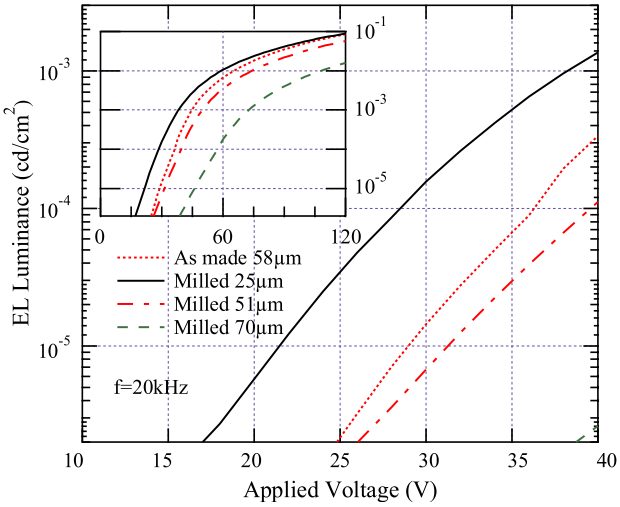

Figure 4. Ac EL luminance as a function of applied voltage at 20 kHz for as-made and 200 RPM for 2 min milled GGL21 phosphors. Dotted line: as-made phosphor, 58 μm thick device; solid line: milled phosphor, 25 μm thick device; dashed-dotted line: milled phosphor 51 μm thick; dashed line: milled phosphor 70 μm thick device. Main figure shows range of maximal enhancement on a semi-logarithmic scale while the inset shows a broader voltage range also on semi-logarithmic scale.

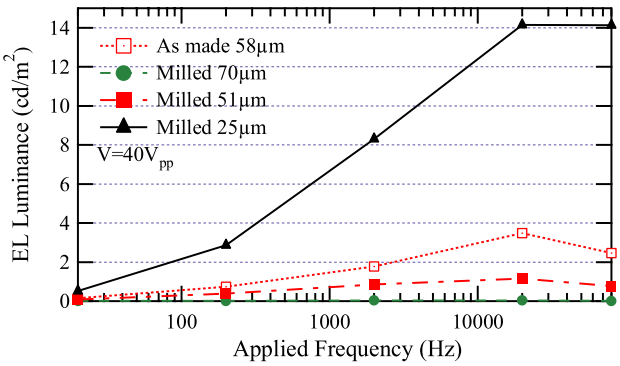

Figure 5. Ac EL luminance as a function of applied frequency at 40 V_{pp} excitation for as-made and 200 RPM for 2 min milled GGL21 phosphor. Dotted line: as-made phosphor, 58 μm thick device; solid line: milled phosphor, 25 μm thick device; dashed–dotted line: milled phosphor 51 μm thick; dashed line: milled phosphor 70 μm thick device.

3. Local structure measurements using EXAFS

We used the EXAFS technique to investigate the extent of any grinding-induced local structure changes about Cu, Zn and Mn in ground materials of ZnS : Cu,Cl (GGL21) and ZnS : Cu,Mn,Cl (GGL11). EXAFS is particularly appropriate for these systems because it can detect small changes in local distortions about very dilute dopants such as 0.15% Cu in these samples. The atom of interest (Cu, Mn or Zn) is selected by using the corresponding x-ray absorption edge for that element.

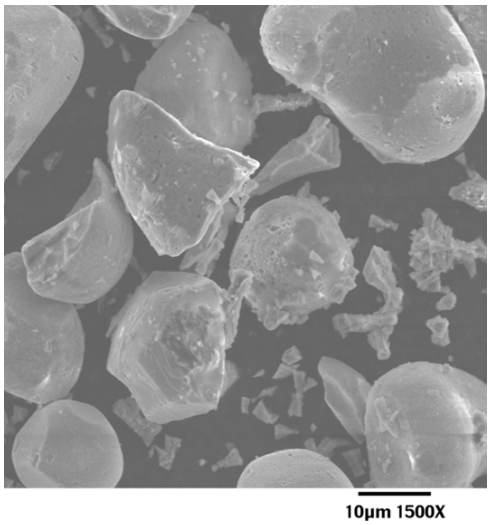

Figure 6. Ground particles viewed using a scanning electron microscope showing a large number of large 10–15 μm particles, a few nearly unground particles, and a few below 3 μm. The ground particles are then size-separated prior to EXAFS analysis.

The first EXAFS experiments were on the as-ground materials discussed above, and indicated that there was increased distortion about the Cu sites. Unfortunately, these first EXAFS results were not conclusive as the amount of distortion varied considerably from sample to sample. However, the SEM images (see figure 6) show that even the heavily ground phosphors contained a mixture of various size particles including a few large particles. Because of the large volume, such particles can dominate over fine particles in EXAFS spectra. In order to have more uniform-sized samples to investigate, the ground particles were size sorted into three groups: large (15–30 μm), medium (3–15 μm) and small (∼1–3 μm).

The size separation process began with four 2 min, 200 RPM grinding cycles each consisting of 1 min of grinding in the planetary micromill and 1 min of cooldown. The particles were then suspended in distilled water and placed in a 1000 mL beaker with a 3 inch magnetic stir bar. The smallest particles were extracted from the top 50% of the solution after letting it sit for 15 min with no stirring; the medium-size particles were extracted while stirring with a vortex of depth 25% of the solution; the large particles were extracted from the remaining, unsuspended powder. Two intermediate extractions were also performed, one between small and medium with stirring but no vortex and one between medium and large with a vortex depth of 50%, in order to provide increased differentiation between the sorted sizes. For the final size-sorted samples for EXAFS analysis, we then used a 25 μm sieve to remove any remaining large particles as they could dominate the EXAFS. In practice, we have found that this sieve passes small particles very well but only a few particles in the 10–25 μm range get though. Most of the size-sorted material was used for the EXAFS samples but a few devices were also made with the smallest particles; they have a very low light output ($\ll$1%), suggesting that there is a size limit below which the individual particles do not luminesce well.

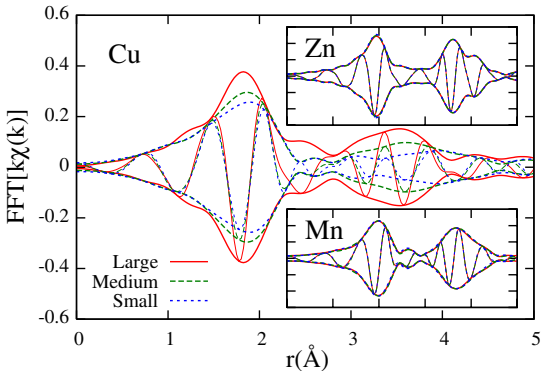

Figure 7. The r-space Cu K-edge EXAFS plots for the three sizes, showing a large peak amplitude decrease for the smaller particles. In the two insets the corresponding results for the Zn host and substitutional Mn (5%) show no change with particle size. Cu and Zn plots for ZnS : Cu,Cl; Mn plot for ZnS : Cu,Mn,Cl. FT ranges: Cu 3.5–11.3 Å; Zn 4.0–13.5 Å; Mn 3.5–13.2 Å.

We therefore conclude that in the devices made with heavily ground but not size-sorted samples, the light emission was likely dominated by the few remaining large particles.

X-ray absorption data were collected at a temperature of 6 K using a liquid helium cryostat, on beamline 10-2 at the Stanford Synchrotron Radiation Lightsource (SSRL). The data were collected in transmission mode for the host Zn K-edge and in fluorescence mode using a 13-element Ge detector for the dopant (Cu and Mn) K-edges. For the Cu K-edge in these low concentration samples (∼0.15% Cu), it is very important to eliminate harmonics that would excite the Zn K-edge, as the host Zn fluorescence can interfere with the very weak Cu fluorescence. This was achieved using a double Si 1 1 1 monochromator (which has no second harmonic) and detuning the monochromator 50% to reduce the higher harmonics. A slit height of 0.7 mm resulted in an energy resolution of ∼1.6 eV. The data were reduced and the k-space files Fourier transformed (FT) to r-space using the RSXAP package [10].

The Cu K-edge EXAFS data presented in figure 7 show a large peak amplitude reduction as the host particle size decreases. We focus on the first peak which corresponds to Cu–S bonds. Since for a Gaussian pair distribution function (PDF) the amplitude is proportional to $1/\sigma$ where σ is the width of the PDF, the decreased amplitude immediately shows an increase of σ for the Cu–S bonds. In contrast, for Zn and Mn K-edge data (shown in the two insets of figure 7), there is no significant change in the amplitudes of any peak, and thus no significant change in σ for the Zn–S or Mn–S bonds. Further, the shoulder on the first peak at ∼2.4 Å for the Cu EXAFS, decreases dramatically as the particle size decreases. This shoulder is a signature for the CuS structure [4] and corresponds to a short Cu1–Cu2 peak; its disappearance indicates that most of the CuS structure is damaged for the smallest ZnS : Cu,Cl particles. This is a very unusual situation because the CuS nano-precipitates (which dominate the EXAFS here because they contains ∼75% of the Cu) are tiny *internal* structures along [1 1 1] planes in the ZnS host. It should also be recognized that in ground particles of most materials, the distortions from grinding are confined

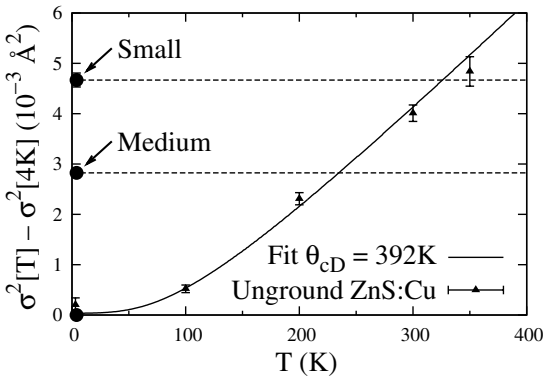

Figure 8. A comparison of σ^2 for Cu–S in different size ground particles at 10 K with previous Cu EXAFS results [5] for unground ZnS : Cu,Cl over a range of T.

to a thin surface layer that is usually a negligible fraction of the sample at micrometre sizes and not observable in EXAFS; surface distortions only become important at the nanoparticle level [11].

To quantify the extent of the distortions for the Cu–S PDF, we fit the first peak of the data two ways: using a theoretical Cu–S standard (FEFF [12]) and using the 4 K data for unground ZnS : Cu,Cl as an experimental standard. The fit range was 1.2–2.1 Å. For each fit only r and σ were allowed to vary and the parameters E_o and S_o^2 were fixed; for the experimental standard, $E_o = 0$ and $S_o^2 = 1$, while for the theoretical standard we fixed these parameters to those used in previous fits [5] $E_o = -8.5$ eV, $S_o^2 = 0.75$. The results from both fits are comparable; the relative increases of σ^2 for the ground samples at 10 K are compared in figure 8 to our previous results for $\sigma^2(T)$ for Cu in unground ZnS : Cu,Cl. For the $\sim 2\,\mu$m particles, the grinding-induced static distortion is comparable to phonon disorder above 300 K.

A further indication of the very large disorder about the Cu atoms is that the shape of the Cu–S peak (in figure 7) becomes quite asymmetric for the smallest particles and the quality of fit parameter C^2 ($\propto$ to χ^2) worsens rapidly as size decreases—for large particles, $C^2 = 13.0$; for medium, $C^2 = 64.9$ and for small, $C^2 = 108.7$; a factor of 8.4 increase compared to the large particles. In contrast, for thermally induced disorder in unground material, the shape of the Cu–S peak changes little and the increase of C^2 from 4 to 300 K is only a factor 2. This large increase of C^2 for the smallest ground samples indicates that describing the grinding-induced disorder by an increased width of either a simple Gaussian or Gaussian broadening the low T data of unground material, is a poor approximation—the grinding-induced disorder is more complex, perhaps a split peak. The fact that the Cu K-edge shows such large effects while the Mn K-edge shows no significant change, means the cleavage of the ZnS particles during grinding is not a random process.

4. Near edge structure

The x-ray absorption near edge structure (XANES) for the Cu K-edge provides yet another probe of the local structure around

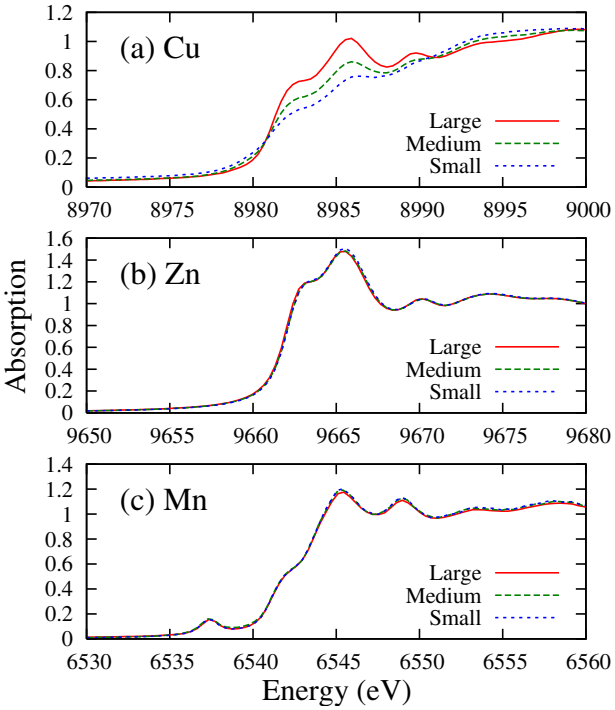

Figure 9. XANES data at the Cu, Zn, and Mn edges as a function of particle size. The Cu XANES data (a) show a significant loss of structure with decreasing particle size; in striking contrast, no change occurs for either the (b) Zn or (c) Mn XANES.

Cu atoms. In general, for very tiny clusters—one or two shells of neighbours—the absorption edge is quite smooth with little structure. Structure in the edge (when it exists) arises from multiple scattering of the ejected photo-electron within a large cluster of order 6–9 Å in radius around the excited atom.

In figure 9, we show the XANES at each absorption edge for three particle sizes. For the host Zn (b) or the dopant Mn (c) XANES there is no significant change in the edge shape which is consistent with the results from the EXAFS analysis, that there is little damage about Zn atoms in the host lattice or about substitutional Mn atoms. In contrast, the Cu K-edge XANES (figure 9(a)) show a large decrease in the edge structure as the particle size decreases, providing further support for preferential damage about the Cu atoms located mainly in the CuS precipitates. These nano-precipitates were initially embedded inside the ZnS host crystallites, and therefore most of them should have remained intact if the grinding process were random. Unfortunately this must remain a qualitative argument as the potentials for sulfides, needed to simulate the Cu K-edge XANES, are not yet good enough [13] for a quantitative comparison.

5. Discussion and conclusions

Decreasing the average particle size is a viable means of producing more light from AC EL devices at a given voltage; however, there are significant limitations to the gains achievable using planetary micro-milling as the EL intensity

decreases surprisingly rapidly as particle size decreases. For 200 RPM milling speeds there is minimal damage so the gains from increasing the average electric field in thinner devices outweigh the decreased EL of the damaged emission centres or precipitates. As milling speeds increase to 400 RPM a larger fraction of the precipitates/emission centres are damaged and the gains due to the increased field cannot compensate for the greatly increased disorder of the Cu precipitates and/or at the Cu emission centres.

Both the EXAFS and the XANES indicate a significant structural change about the Cu atom within the CuS precipitates when the ZnS : Cu,Cl or ZnS : Cu,Mn,Cl phosphor particles are ground to make fine particles, yet no corresponding change is observed for the Zn host material or the Mn dopant in ZnS : Cu,Mn,Cl. Note that the changes in the Cu K-edge data are nearly the same in both ZnS : Cu,Cl and ZnS : Cu,Mn,Cl (not shown). This means that the CuS precipitates, initially embedded inside the ZnS : Cu,Cl particles, are preferentially damaged while the ZnS material surrounding them is not—a very unusual situation. The only way that the CuS nano-precipitates can be significantly damaged without noticeable damage to the ZnS host in the grinding process are: (1) the ZnS particles cleave along [1 1 1] planes containing the CuS precipitates, thereby fracturing the tiny CuS nano-precipitates or (2) the ZnS particles crack or are badly strained along these planes. Note that an 18.4 Å thick layer of CuS (one unit cell c axis parameter plus one S–S double bond) can replace a region of ZnS in a [1 1 1] plane that is 18.7 Å thick (twice the cube diagonal of the cubic unit cell) as shown in figure 10, producing a small strain of 1.6% between the two materials. More importantly, along the interface-layer the strain is even smaller; the S–S distance in the ab plane for CuS is 3.80 Å while the S–S distance in the [1 1 1] plane for ZnS is 3.825 Å, a strain of only 0.66%. This small strain will allow epitaxial growth between the two crystal structures. From our earlier EXAFS studies [4] we had suggested that the CuS precipitates are likely epitaxially bonded to the ZnS host; figure 10 thus provides a reasonable explanation for this observation. In addition, recent results show that etching occurs preferentially through the [1 1 1] planes in ZnS : Cu [14], suggesting that the ZnS [1 1 1] planes are indeed weakened by the presence of the CuS nano-precipitates.

We suggest that fracturing through the CuS nano-precipitates is more likely because the CuS would then be left in the surface layer on the outside of the ZnS particles where it would rapidly become more disordered by further grinding. Note that CuS is a layered structure with S–S double bonds that may break easily under strain. In addition, the fact that the AC EL nearly disappears when we damage primarily the CuS nano-precipitates strongly reconfirms the idea that the CuS nano-precipitates are crucial for relatively low voltage AC EL. However we must note one caveat: because the PL also decreases qualitatively for ground samples the Cu emission centres might also be damaged. One possible explanation is as follows. The samples are prepared by quenching the phosphors from high temperatures. As the cubic phase develops, the Cu precipitates develop along [1 1 1] planes—but there then might be a cloud of Cu centres close to the precipitates

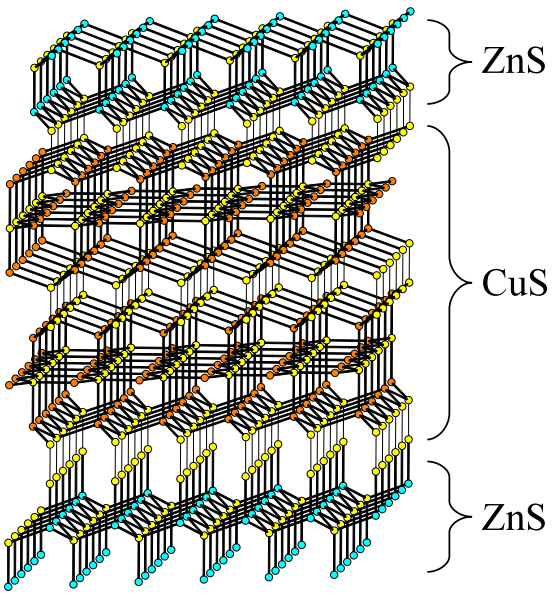

Figure 10. The CuS nano-precipitate fits into the [1 1 1] planes of the ZnS host with 1.6% tensile strain; the vertical height of the CuS slice is 18.4 Å instead of 18.7 Å for the ZnS structure. The vertical axis is the cubic [1 1 1] direction for ZnS.

that become frozen in place as the sample rapidly cools, i.e. the distribution of Cu defects may not be uniform but are more concentrated close to some [1 1 1] planes. In that case, cleaving along such [1 1 1] planes that contain the CuS precipitates may also damage the Cu emission centres or place them at the surface where non-radiative processes may quench the light emission. Further work is necessary to determine whether or not the Cu defect distribution is uniform at the nanoscale.

Despite the size limitation of micro-milling, the enhancement of light output at lower voltages for the 25 μm thick devices compared to the standard 50 μm thick device is interesting due to the significant number of applications that utilize AC EL phosphors for illumination in the mcd cm^{-2} range, including back lighting for passive LCDs. To produce 1 mcd cm^{-2} with the thinner device in this study requires 15% less voltage, increasing the attractiveness in low intensity applications where the requirements for higher applied voltages are often a significant hindrance. To produce ZnS : Cu,Cl AC EL devices that utilize the field enhancement from CuS precipitates thinner than 10 μm, a fabrication approach from colloidal nanoparticles [15] will probably be more successful.

Acknowledgments

The work at UCSC was supported by DOE Basic Energy Sciences grant DE-FG02-07ER46388. The EXAFS/XANES experiments were performed at SSRL (operated by the DOE, Division of Chemical Sciences, and by the NIH, Biomedical Resource Technology Program, Division of Research Resources).

References

[1] Destriau G 1936 Experimental studies on the action of an electric field on phosphorescent sulfides *J. Chem. Phys.* **33** 620

[2] Fischer A G 1962 Electroluminescent lines in ZnS powder particles *J. Electrochem. Soc.* **109** 1043

[3] Fischer A G 1963 Electroluminescent lines in ZnS powder particles: II. Models and comparison with experience *J. Electrochem. Soc.* **110** 733–48

[4] Warkentin M, Bridges F, Carter S A and Anderson M 2007 Electroluminescence materials ZnS : Cu,Cl and ZnS : Cu,Mn,Cl studied by EXAFS spectroscopy *Phys. Rev.* B **75** 075301

[5] Stanley J, Jiang Y, Bridges F, Carter S A and Ruhlen L 2010 Degradation and rejuvenation studies of AC electroluminescent ZnS : Cu,Cl phosphors *J. Phys.: Condens. Matter* **22** 055301

[6] Nien Y-T and Chen I-G 2006 Raman scattering and electroluminescence of ZnS : Cu,Cl phosphor powder *Appl. Phys. Lett.* **89** 261906

[7] Shionoya S 1999 *Phosphor Handbook* (New York: CRC Press) pp 231–58 chapter 3

[8] Wood V, Halpert J E, Panzer M J, Bawendi M G and Bulovic V 2009 Alternating current driven electroluminescence from ZnSe/ZnS : Mn/ZnS nanocrystals *Nano Lett.* **9** 2367–71

[9] Faria S 1988 Electroluminescent characteristics of small particle size phosphors *J. Electrochem Soc.* **135** 2627

[10] See http://lise.lbl.gov/RSXAP/

[11] Gilbert B, Huang F, Zhang H, Waychunas G and Banfield J 2004 Nanoparticles: strained and stiff *Science* **305** 651–4

[12] Ankudinov A L, Ravel B, Rehr J J and Conradson S D 1998 Real space multiple scattering calculation of XANES *Phys. Rev.* B **58** 7565

[13] Rehr J J 2010 private communication

[14] Withnall R, Silver J, Ireland T G, Fern G R and Marsh P J 2009 Structure and morphology of ACEL ZnS:Cu,Cl phosphor powder etched by hydrochloric acid *J. Electrochem. Soc.* **156** J326

[15] Manam J, Chatterjee V, Das S, Choubey A and Sharma S K 2010 Preparation, characterization and study of optical properties of ZnS nanophosphor *J. Lumin.* **130** 292–7